Mitigation of Transient Ground Potential Rise in Gas Insulated Substations during Very Fast Transient Overvoltage

***Muresan Alexandru*[1,2], **Levente Czumbil*[1,2], *Alexis Polycarpou*[3], *Hassan Nouri*[4], *Roberto Andolfato*[5], **Dan D. Micu*[1,2]**

[1]Energy Transition Research Center, Technical University of Cluj-Napoca, Cluj-Napoca, 400027, Romania

[2]Department of Electrotechnics and Measurements, Faculty of Electrical Engineering, Technical University of Cluj-Napoca, Cluj-Napoca, 400027, Romania

[3]Frederick University, Nicosia, 3080, Cyprus

[4]Power Systems Research Laboratory, University of West England (UWE), Bristol BS16 1QY, UK

[5]SINT Srl, 36061 Bassano del Grappa, VI, Italy

*Correspondence: Levente Czumbil (LC), levente.czumbil@ethm.utvluj.ro;
Dan Doru Micu (DDM), dan.micu@ethm.utcluj.ro

ABSTRACT

This paper is focused on the assessment and mitigation of the transient response of a Gas Insulated Substation's (GIS) grounding grid to the fault due to voltage breakdown using the Partial Element Equivalent Circuit (PEEC) numerical approach. The adopted analysis methodology considers the magnetic induction by quantifying the electromagnetic couplings generated within the metallic components contained by the GIS configuration. The Transient Ground Potential Rise (TGPR) and transient current are computed and analyzed at several locations inside of GIS housing. With the aid of 3D graphical representation, the maximum amplitudes of the TGPR across the substation are illustrated. The mitigation efforts are considerably optimized by assuming the grounding grid sub-system is responsible for high frequency fault energy clearance based on identification method. By adopting several simplifications of the earthing system during the computational process, from a step-by-step analysis, it has been discovered that the grid located beneath the GIS enclosure will mostly attenuate the TGPR across the GIS building. Based on the aforementioned findings a successful mitigation technique is implemented.

NOMENCLATURE

AIS – Air Insulated Substation;
CAD – Computer Aided Design;
DE – Differential Equation;
EMF – Electro-Magnetic Field;
FDTF – Finite Difference Time Domain;
FEM – Finite Element Method;
GIS – Gas Insulated Substation;
GISw – Gas Insulated Switchgear;
HALD – the proposed equivalent co-axial cable model implemented in PSCAD for the investigated GIS section; named with regard to the first name of the four authors how developed this approach: H. Nouri, A. Muresan, L. Czumbil and D.D. Micu;
HV – High Voltage;
IE – Integral Equation;
MoM – Method of Moments;
PEEC – Partial Element Equivalent Circuit;
TGPR – Transient Ground Potential Rise;
VFTO – Very Fast Transient Overvoltage;

I. INTRODUCTION

The changing dynamics of human migration towards metropolitan areas implies a fast development of local emerging economies which will result in higher installed power demands in specific locations inside crowded metropolitan areas worldwide. As a consequence, the industry, specifically electrical equipment manufacturers, must adapt to the energy demand changing needs and deliver suitable technical solutions. One of the major challenges arising when additional installed power needs to be delivered towards crowded areas across major cities is the lack of available land required for new substations to be installed. Making an analogy with the solution found by construction scientists and urbanists, who build vertically where a lack of space does not allow another approach, an innovative and efficient solution has been developed by electrical engineers, namely Gas Insulated Switchgear (GISw) technology. Although GISw technology contains sulfur hexafluoride (SF6) [1, 2] as a dielectric medium which is considered a toxic gas for the human body and the environment, a study conducted by Alstom Grid based on 18 environmental indicators shows that if long-term (40 years) analysis is employed the Air Insulated Substation (AIS) technology has a greater impact on the environment compared to equipment encapsulated in SF6 gas [3]. The amount of aluminum used in the construction of the two substations is directly proportional to the allocated land area [3].

Gas Insulated Substations (GIS) are subjected to very high-frequency transient regimes due to switching operations during steady state and transient regime [4-9]. According to several studies presented in the literature, the Very Fast Transient Overvoltage (VFTO) leaks towards the metallic enclosure at the flanges located between two particular enclosures, at the air-SF6 bushing and during the voltage breakdown fault between a phase conductor and metallic enclosure [10-13]. It has been found based on many VFTO measurements in laboratories and actual GISs that the VFTO frequency range varies from a few MHz up to 100 MHz with amplitudes ranging 1.2 p.u. to 3.0 p.u. on the core conductor of the GIS and 0.1 p.u. to 0.7 p.u. on the metallic enclosure (pipe) [14-18]. Considering that the metallic enclosure is galvanically connected to the substation grounding grid through the grounding leads (with minimum of one connection between enclosure and the earthing system) these transients flow towards the grounding grid back and forth affecting the overall performance of the earthing system. Moreover, Transient Ground Potential Rise (TGPR) will occur across the substation due to the malfunction of the grounding grid coordination.

Description of the problem

The performance of the grounding grid during transient regimes is greatly affected by high frequencies VFTO. The common grounding grid designing procedures follow the IEEE 80-2013 Std. [19] which takes into consideration only the power frequency fault currents. The VFTO is briefly mentioned under theoretical aspects and recommendations. Furthermore, an inherent conceptual paradox occurs in the case of the grounding grid designing procedures associated with GIS substations, which, in principle, contradicts the conventional designing methodology that governs conventional stations and substations: in general, a complex grounding system increases the capabilities of the protection system to clear the fault energy. Contrary, when a Gas Insulated

Substation is subjected to very fast transients the effective area of the grid is significantly reduced (the grounding grid sub-system responsible for fault energy clearance) and the overall performance of the grounding grid is affected, mainly due to the fast time distribution of the transient electromagnetic wave. The effective area (or effective radius) of the grid is an important parameter that one needs to take into consideration when designing an optimum grounding system [20]. The concept of the effective area of the grid indicates that the impulse impedance dissipates along the grid area before reaching the other end [20]. Therefore, only a part of the grid is effective to scatter the transient discharged current/voltage [19-22]. When the low-frequency impulse impedance of the grid is higher than its impulse impedance the entire grid is efficient in dissipating the fault energy [19-22]. Moreover, based on several electromagnetic field-based modeling techniques, a dependence between the time distribution of the fast-transient phenomena and the effective area of the grounding grid is illustrated considering several lightning current waveforms [23]. Based on the conclusions presented in the maximum amplitude of the Transient Ground Potential Rise is inversely proportional to the rise time parameter of the lightning waveform, as well as the effective area of the grounding grid. Therefore, a faster transient wave will produce higher amplitudes of TGPR concentrated on smaller areas across the grid. However, the study contains a simplified rectangular grounding grid composed of only the underground conductors that are subjected only to fast transients (frequency up to 1 MHz) disturbances.

Ideally, the most effective mitigation technique for controlling the very fast transient would be through use of a metallic plate which is rather expensive. It is important to highlight that when such complex configurations of metallic conductors need to be evaluated as GIS metallic arrangements, the analytical and empirical formulas cannot be applied. Furthermore, the existing modelling techniques cannot assess the overall transient response of the substation during high frequency voltage breakdown. Hence, a more accurate analysis is required in order to correctly quantify the real transient response of a complex GIS configuration during very fast transient overvoltage.

The current paper tries to answer to this requirement by presenting a simulation technique the allow to take into account the complex 3D structure and the various electromagnetic coupling phenomena that take place between the metallic structure of a real GIS and the associated earthing system during VFTO events. The proposed GIS modeling and simulation technique is applied in case of 110 kV GIS in order to identify the grounding grid area that mostly effect the clearance of VFTO fault. Finally, a mitigation procedure is show cased for the identified grounding grid area in order to accelerate the clearance of VFTO faults.

Therefore, after this introductory part the paper is structured as follows: in the second section, the theoretical and mathematical background of the paper are presented alongside the identification of the problem. Also, in the second section, the geometrical approach adopted by the authors is described and validated through a rigorous endorsement procedure. In the first sub-section of the third section, the Transient Ground Potential Rise across the GIS building (or housing) is evaluated considering several locations. The following two sub-sub sections deal with the identification of critical areas of the grounding grid alongside the implementation of a mitigation technique impacting the TGPR. The conclusions are presented in the fourth section.

II. MODELING METHODOLOGY

A. State of the art regarding applied modelling techniques

The first case studies regarding Gas Insulated Substation equivalent models date back to 1996 and follow the widely known circuit theory approach [24, 25]. The methodology is based on representing the system under study with equivalent circuit elements, lumped parameters, or transmission line coefficients (propagation speed, length, mathematical model, etc.) [13, 26]. The circuit formulation methodology follows Kirchhoff's laws, embedded in different software interfaces, providing numerical solutions for an energy system operating at a known voltage level, however it neglects the electric and magnetic field in the direction of propagation [27].

The circuit theory approach has proven to be an efficient analysis tool for the GIS in terms of accurately identifying the level of VFTO generated across the substation during switching events. A comprehensive study of circuit theory approach modeling procedures applied to Gas Insulated Substations can be found in [11]. With this approach, several drawbacks exist when applied to complex configurations of a GIS under very fast transient events. Firstly, the complex three-dimensional geometries cannot describe or compute the spatial distribution of the fault current and voltages (e.g. identifying critical locations of step and touch voltages across a grounding grid). Secondly, when the wavelength of the fastest transient electromagnetic wave is comparable with the physical dimensions of the system, then, the retarded potentials need to be considered during the computational process. There are several other related GIS issues which will not be covered here.

The alternative solution is to represent by the Electro-Magnetic Field (EMF) numerical methods which have gained acknowledgment in recent years due to improved computing capabilities.

Table 1. Summary of electromagnetic numerical approaches applied to GIS analysis

Ref No	Numerical Method	Fault Type	Analysis Type	Applied Software package
[23, 28-30]	MoM	Power Frequency Fault	Step and Touch Voltage	CDEGS
[31]	MoM	Switching Events	Transient EMF	Not mentioned
[32, 33]	MoM	Partial Discharge	PD Analysis	Not mentioned
[34-37]	FEM	Breakdown voltage	Dielectric strength	ANSYS
[38, 39]	FEM	Partial Discharge	Electric Field distribution	ANSYS COMSOL
[40-43]	FDTD	Partial Discharge	PD Analysis	Not mentioned
[44]	FDTD	Steady state	VFT Analysis	Not mentioned
[45]	FDTD	Voltage breakdown between DS contacts	EMF Analysis	Not mentioned
[46-48]	FDTD	Switching events	EMI Interference	Not mentioned
[8]	PEEC	Shell circulating currents	EMF Analysis	ATP-EMTP
[51, 52]	PEEC	Voltage Breakdown	TGPR across substation	XGSLab

Different from the aforementioned circuit theory approach, EMF numerical methods can deal with very complex geometries regardless of the physical dimensions of the system under study. Full-Wave numerical electromagnetic analysis methods are defined as methodologies allowing the direct numerical solution of Maxwell's equations in both frequency and time domain [27]. Maxwell's equations can be expressed in the Differential Equation (DE) form and Integral Equation (IE) form from which several numerical approaches have been developed over time [27]. DE based methods require the discretization of the entire computational domain's volume. This approach leads to a high amount of computational resources, thus imposing limitations regarding the analysis of large complex geometries. On the other hand, the IE based numerical methods can deal with large geometries, whose digital avatars are developed using CAD software, since the discretization algorithms are applied only on the metallic structures (MoM - superposition principle and PEEC - thin wire assumption). The most commonly used numerical approaches in solving Maxwell equations, applicable to gas-insulated substation analysis, are Method of Moments (MoM) [28-33], Finite Element Method (FEM) [34-39], Finite Differences Time Domain (FDTD) approach [46-48] and the Partial Equivalent Element Circuit (PEEC) method [8, 51, 52] briefly structured in Table 1.

The adopted modeling philosophy is based on a PEEC approach, which provides a full wave solution, under the interface of XGSLab software package [49]. In the following section the mathematical background of the numerical algorithm is presented and discussed. The PEEC numerical approach has been previously applied towards GIS analysis in [8] however using the algorithms only for computations of equivalent circuit elements as inputs of Electro-Magnetic Transient Program (EMTP) model.

B. Mathematical Background, Partial Equivalent Element Circuit Method (PEEC)

The Partial Equivalent Element Circuit (PEEC) method is a hybrid IE technique, it is based on the Mixed Field Integral Equation from which an equivalent circuit is extracted, and it does not require discretization of the whole domain space. The implemented PEEC method solves the Maxwell equations in full wave conditions considering the Green functions for propagation, the Sommerfeld integrals for the earth reaction, the Jefimenko's equations for electric and magnetic fields and moving from the frequency to the time domain by means of Fourier transforms [49].

For a Gas Insulated Substation complex metallic enclosure and its adjacent metallic structures, the method will divide the model in small current (charge) and potential cells as will be further presented. During the present study the PEEC numerical method has been adopted under the software interface XGSLab developed by the Italian company SINT, Bassano del Grappa.

In this regard, a frequency domain general approach of PEEC hybrid method is presented (by R. Andolfato) starting from the following equation, assuming a thin wire:

$$\left(\overrightarrow{E_e} + \vec{E}\right) \cdot \vec{\ell} = (z_i + z_c) \cdot I \cdot \vec{\ell} \tag{1}$$

where $\vec{E}$ is the tangent electric field at the conductor surface, $\overrightarrow{E_e}$ is an incident electric field or a generator, z_i represents the internal impedance of the conductor and z_c the impedance of the

coating (assuming the conductor is coated), I is the current flowing along the conductor and $\vec{\ell}$ is axial unit vector tangent to the conductor surface.

Because the thin structure approximation, equation (1) can be rewritten considering only the axial components along the conductor. The following scalar equation on the conductor surface results:

$$E = (z_i + z_c) \cdot I - E_e \tag{2}$$

Due to the charges and currents axial distributions along the conductor, the electric field $\vec{E}$ outside the conductor is related with the scalar potential V and vector potential $\vec{A}$ according to following equation:

$$\vec{E} = -gradV - j\omega\vec{A} \tag{3}$$

Considering the thin wire approximation, the (3) can be written as follows:

$$E = \frac{\partial V}{\partial l} - j\omega A \tag{4}$$

Combining equations (1) and (4) yields:

$$(z_i + z_c) \cdot I + j\omega A + \frac{\partial V}{\partial l} = E_e \tag{5}$$

The forcing term E_e can represent an incident or a generator field. Further, by dividing the vector potential in self A_s and mutual A_m components as well assuming that the self-component A_s on the conductor surface correspond to its external impedance z_e, equation (5) can be expressed as:

$$(z_i + z_c) \cdot I + j\omega A_s + j\omega A_m = (z_i + z_c) \cdot I + z_e \cdot I + j\omega A_m = z_s \cdot I + j\omega A_m \tag{6}$$

By adopting the aforementioned procedure, the self-impedance term z_s not only contains the external components, but also internal and coating impedances. Considering a real configuration of a certain metallic structure, the system must be fragmentated in short elements in order to implement the previous relations in a numerical model (composed of current and potential cells). For a current cell i with the length l_i and the point i_+ and i_- the integral of (5) can be written:

$$\int_{l_i} \left(z_{si} \cdot I_i + j\omega A_m + \frac{\partial V}{\partial l} \right) dl = \int_{l_i} E_e dl \tag{7}$$

Considering the current distribution assumption:

$$z_{si} \cdot l_i \cdot I_i + j\omega \int_{l_i} A_m dl + V_{i+} - V_{i-} = \int_{l_i} E_e dl \tag{8}$$

For each current cell j with the length l_j the mutual magnetic potential A_m can be mathematically described as follows:

$$A_m = \frac{\mu}{4\pi} \cdot \sum_{j \neq i} \left(I_j \cdot \cos \varphi_{ij} \cdot \int_{l_j} \frac{e^{-\gamma r}}{r} dl \right) \tag{9}$$

Considering the complementary potential cell k with the length l_k the scalar potential can be expressed as follows:

$$V_{i*} = \frac{1}{4\pi\dot{\sigma} l_{i*}} \cdot \sum_{k} \left(\frac{J_k}{l_k} \cdot \int_{l_{i*}} \int_{l_k} \frac{e^{-\gamma r}}{r} dl_k \, dl_{i*} \right) \tag{10}$$

The sum term from (10) is extended to all potential cells adopting the following conditions:

$$z_{si} \cdot l_i \cdot I_i = Z_{si} \cdot I_i \tag{11}$$

$$j\omega \int_{l_i} A_m dl = j\omega \cdot \frac{\mu}{4\pi} \cdot \sum_{j \neq i} \left(I_j \cdot \cos \varphi_{ij} \cdot \int_{l_i} \int_{l_j} \frac{e^{-\gamma r}}{r} dl_j \, dl_i \right) = \sum_{j \neq i} \left(Z_{mij} \cdot I_j \right) \tag{12}$$

$$V_{i_+} = \frac{1}{4\pi\dot{\sigma} l_{i_+}} \cdot \sum_{k} \left(\frac{J_k}{l_k} \cdot \int_{l_{i*}} \int_{l_k} \frac{e^{-\gamma r}}{r} dl_k \, dl_{i*} \right) \tag{13}$$

$$V_{i_-} = \frac{1}{4\pi\dot{\sigma} l_{i_-}} \cdot \sum_{k} \left(\frac{J_k}{l_k} \cdot \int_{l_{i*}} \int_{l_k} \frac{e^{-\gamma r}}{r} dl_k \, dl_{i*} \right) \tag{14}$$

$$\int_{l_i} E_e dl = E_{ei} \tag{15}$$

$$Z_{mij} = j\omega \cdot \frac{\mu \cdot cos\varphi_{ij}}{4\pi} \int_{l_i} \int_{l_j} \frac{e^{-\gamma r}}{r} dl_j \, dl_i \tag{16}$$

$$W_{ij} = \frac{1}{4\pi\dot{\sigma} l_i l_j} \cdot \int_{l_i} \int_{l_j} \frac{e^{-\gamma r}}{r} dl_j \, dl_i \tag{17}$$

The previous equations (11)-(17) along the current cell can be expressed as follows:

$$Z_{si} \cdot I_i + \sum_{j \neq i} \left(Z_{mij} \cdot I_j \right) + \sum_{k} \left(W_{i_+k} \cdot J_k \right) - \sum_{k} \left(W_{i_-k} \cdot J_k \right) = E_e \tag{18}$$

The application range of the method is greatly dependent upon the accuracy of the computational process regarding Z_m, Z_s, W_s and W_m (W_s, W_m represent the self and mutual coefficient of potential of a single or between a couple of elements).

The time domain solution is obtained by applying the forward and inverse Fourier Transform, FFT-PEEC-IFFT. Considering the harmonic impedance concept, it is possible to compute the transient response in time domain for a certain metallic configuration. The transient

response of a Gas Insulated Substation configuration that includes the grounding grid, to a transient energization voltage or current can be computed from the following relation:

$$u(t) = F^{-1}[Z(f)I(f)] = F^{-1}[Z(f)F(u(t))] \quad (19)$$

By using the Inverse Fast Fourier Transform it is possible to compute current, leakage current and potentials across the system (on any particular element). In order to optimize the computational process, the algorithm considers only a set of representative frequencies per decades with a growing density with frequency. The discretization of the implemented model is strictly dependent on frequency of the transient source and on propagation medium. Therefore, the maximum length of an element must be lower than $1/6$ of the wavelength. Considering the very fast time distribution of the adopted transient source (voltage) during the computational process, the maximum length of the elements is set to be $0.19\ m$.

C. Geometrical approach

The basic modeling concept is presented in [51]. Figure 1 illustrates, for explanatory purposes, the adopted geometrical assumption in comparison with the real case scenario (solid co-axial pipe). The GIS co-axial enclosure is represented by six parallel aluminum bars having a thickness considered to be equal with the distance between the inner and outer wall of the GIS enclosure accounting also for the thickness of both metallic walls.

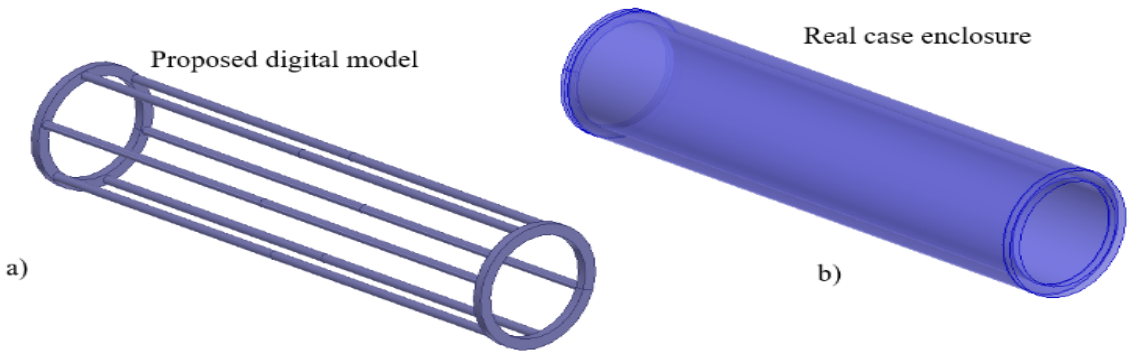

Figure 1. Computer-aided design model

Proof of concept, validation

In order to validate the previously adopted geometrical concept, a validation procedure is developed by comparing the Transient Ground Potential Rise recorded in the middle of the metallic enclosure using two different modeling concepts: circuit theory approach (using PSCAD software [50] which applies a quasi-TEM approach for cable modeling) and electromagnetic field theory approach (using XGSLab software package [49] which applies a PEEC numerical approach). A simplified case study is built containing 2 m of horizontal GIS enclosure, 1 phase conductor, and 20 m of incoming aerial cable. The GIS enclosure is connected in four points at the grounding grid, which is modeled through four equivalent resistors, $R = 1\ m\Omega$ (see Figure 2).

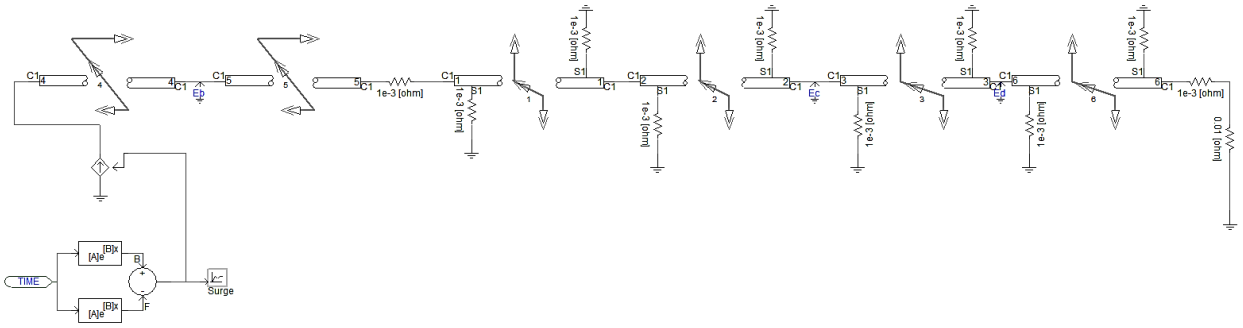

Figure 2. PSCAD implemented proof of concept validation circuit

A voltage breakdown fault is assumed in the middle of the enclosure due to a lightning fault current on GIS conducting core. When the circuit theory approach is employed, the metallic enclosure and its contents is modeled through a coaxial cable interface, named the HALD model (see Figure 3), where the core of the cable represents the phase conductor, the first insulating layer the dielectric material (air or SF6), and the cable sheath represents the GIS enclosure. It is crucial that the total impedance of the system be computed in order to set a matching impedance as load to avoid artificial reflections. Moreover, similar to representing the GIS arrangement through equivalent circuit elements the method cannot encompass three-dimensional geometry.

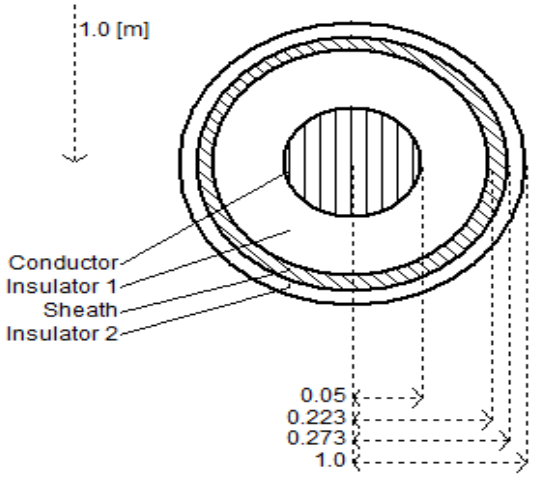

Figure 3. Applied "HALD" 4-layer co-axial cable model for the test GIS section implemented in PSCAD

Three scenarios of transient analysis on GIS section were performed with a double exponential function lightning surge pulse model with constant amplitude but three different rise and fall times (see Figure 2). Figure 4 represents the TGPR waveforms obtained through the electromagnetic field PEEC model in XGSLab and circuit theory HALD model in PSCAD for a 30 kA $1/50$ μs lightning fault current.

The average percentage error between the computed results is less than 6 %, see Table 2 and Figure 4, higher error values being recorded after the 5th cycle when the TGPR waveform amplitude is significantly reduced (under 20 % from the amplitude of the 1st TGPR waveform cycle) and therefore do not affect protection design processes.

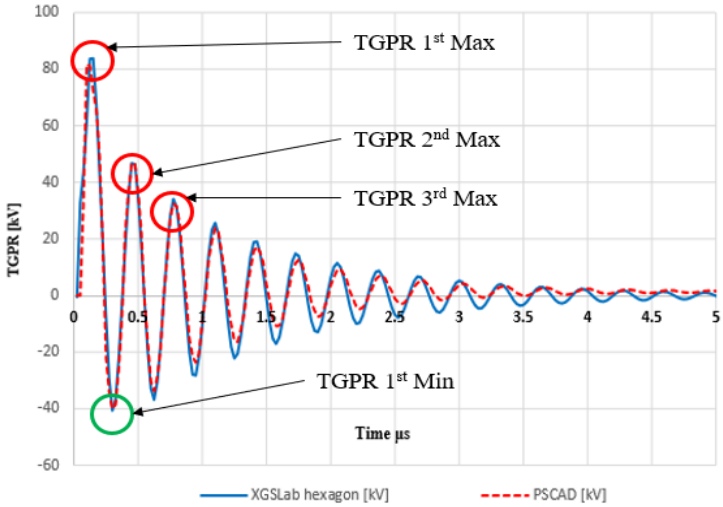

Figure 4. TGPR recorded in the middle of the enclosure through both methodologies

Table 2. Numerical comparison of the maximum TGPR values computed during in first 7 transient state waveform cycles

Max TGPR [kV]	HALD [kV]	EMF [kV]	Error [%]
TGPR 1st Max.	81.71	83.76	**3%**
TGPR 1st Min.	-40.01	-40.64	**2%**
TGPR 2nd Amp.	46.83	46.34	**1%**
TGPR 3rd Amp.	32.5	34.1	5%
TGPR 4th Amp.	23.9	25.6	7%
TGPR 5th Amp.	17.6	19.1	9%
TGPR 6th Amp.	12.8	14.8	16%
TGPR 7th Amp.	9.5	10.1	6%
Avg. Error [%]	5.96%		

The mathematical stability and linearity of the implemented EMF and HALD models were tested by increasing the lightning current amplitude with a factor of 2, errors in acceptable limits were recorded. Moreover, to compute TGPR at several locations along the investigated GIS component the implemented models were slightly modified. In the case of the circuit theory approach, the HALD cable model was divided into 0.5 m long sections (see Figure 2), while in the case of the electromagnetic field approach model the parallel aluminum bars used for GIS enclosure were subdivided into 4 spans. Similar, subdivision techniques were applied for the incoming power cable in both models. The TGPR was recorded at 0.5 m, 1 m and 1.5 m distance across GIS simplified enclosure. The average TGPR evaluation error maintains in acceptable limit, around 6 % for all the investigated GIS enclosure locations. The dielectric material surrounding the phase conductor in the first case study, is considered to be air and in the second case study SF6 gas (see Figure 3). The recorded TGPRs in the middle of the enclosure for both case studies are

similar. Hence, it can be stated that during the voltage breakdown fault the galvanic coupling dominates the transient response of the GIS enclosure.

In [52] the validated concept was successfully applied to a real configuration of Gas Insulated Substation. One of the purposes of the study presented and performed in [52] was to quantify how the different number of parallel aluminum bars representing the solid metallic pipe will impact the transient response of the enclosure during voltage breakdown fault, taking into account very-high-frequency transients [52]. The average errors computed from the numerical values of maximum and minimum amplitudes measured from the first through fourth periods of the waveform which were between acceptable limits, i.e. 2–5 % [52]. The spatial distribution of the aluminum bars surrounding the phase conductor is slightly different for each model, however a similar transient response of the model was recorded regardless of the geometric approach adopted. Due to geometric symmetry reasons as well as from a computational time point of view, the hexagon-based geometry was developed and further used for the real GIS model analysis [52].

III. CASE STUDY

The system under study is a $110\ kV$ GIS substation in three-phase configuration in the same GIS enclosure, located in a dedicated building, see Figure 5. The substation is fed from two $220/110\ kV$ autotransformers represented in the model through two equivalent impedances $Z_{AT1} = Z_{AT2} = 0.1\ \Omega$. Because of the nominal voltage rating of the system, the three phase conductors are located inside of one co-axial pipe in a radial configuration with respect of the geometric origin of the metallic shell. In order to ensure the redundancy characteristic of the feeder, the double bus configuration is considered. The substation is composed from eight modules labelled BS1 to BS8 and a bus coupler. The bus coupler is located in the middle of the enclosure which facilitates the switching from BS1 to BS8 (see Figure 5).

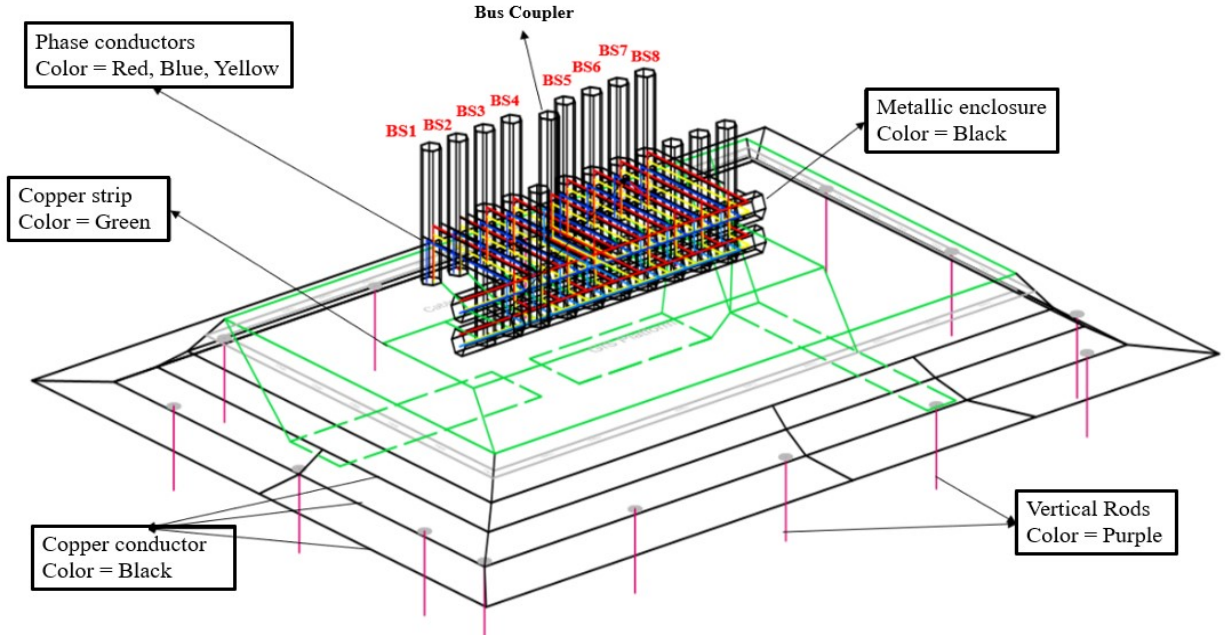

Figure 5. 110 kV GIS substation model, CAD top view

Each GIS module enclosure is connected to a copper strip ring (located on the GIS concrete platform) in two locations through copper grounding leads. An additional copper strip ring is located on the inner wall of the GIS building at $h = 0.3\ m$. In order to reduce the touch and step voltages at power frequency fault, four copper conductor rings are located outside of the GIS building at different depths with respect to the soil surface. At equidistant points across the third copper conductor ring, 13 vertical rods are connected. Considering the very fast nature of this study (wavelength comparable with the physical length of the system) the apparatus located outside of the GIS building has been not considered during the computational process. The geometrical characteristics and the implemented materials adopted during the computational process are presented in Table 3.

Table 3. Geometric characteristics of the model components.

Model Component	Diameter d [mm]	Conductor Material
Phase conductor	30	Copper
aluminum Bar	40	aluminum
Copper strip	28.65	Copper
Copper conductor	12.36	Copper
Vertical rods	20	Copper

Elements not having a cylindrical cross-section need to be represented with an equivalent cylindrical configuration. In general, the equivalent element must have the same admittance to earth and the same self-impedance of the actual element [19]. Based on the relations presented in [19] the copper strip is modelled as an equivalent cylindrical conductor with similar outer surface. The pure resistive loads that are assumed during the computational process, modelled as transversal impedances to earth connected at each phase conductor. The modelling scenario assumes phase-to-enclosure fault as a galvanic connection between the phase conductor and the aluminum bar. For simulation purposes the transient overvoltage scenario is performed with a double exponential pulse generator that has $1\ p.u.$ of fault overvoltage amplitude ($1\ p.f.u.$), and $10\ ns/3\ \mu s$ rise and fall time. The focus is not on the applied overvoltage amplitude that cases the phase-to-enclosure fault but on presenting a proper way to model the metallic structures correlated to Gas Insulated Substation and to identify effective area of the grounding grid that influence TGPR distribution in case of VFTOs in order be able to properly design the earthing system for such phenomena as well.

The double exponential pulse generator is expressed as:

$$V(t) = V_m(e^{-\alpha t} - e^{-\beta t}) \qquad (20)$$

where $\alpha = 2.31049 \cdot 10^5\ \text{sec}^{-1}$, $\beta = 8.17350372 \cdot 10^9\ \text{sec}^{-1}$, and $V_m = 1$ p. f. u.

The transient source is located inside the BS6 enclosure, which is also assumed to be the faulted bus. By means of Fast Fourier the time domain signal is transformed in frequency domain. The software will divide the frequency spectrum in several frequency decades containing a limited number of representative frequencies. The response of the system is computed for each representative frequency following the construction of the solution in time domain by means of Inverse Fourier Transform (IFT). During the present study 192 of representative frequencies have been used during the computational process.

The main purpose of the analyzed case study is to assess the transient response of the grounding grid in order to identify the proper location across the earthing system where the mitigation techniques should be applied. By identifying areas of the grid, the financial and constructive efforts entailed by further attenuation measures will be optimized.

A. Assessment methodology

The study aims to investigate the real transient response of a typical Gas Insulated Substation configuration (see Figure 5) based on which the effective area of the grounding will be identified. Furthermore, a proper mitigation technique will be implemented by decreasing the resistance of the grounding grid located beneath the GIS enclosure. Several analysis locations across the GIS building are established in which the TGPR and the transient current are computed, highlighted with blue dots in Figure 6. In order to quantify how different sub-systems of the grounding grid act in controlling the very fast transients flowing throughout the substation, the earthing system will be gradually simplified. With each adopted simplification the TGPR and transient current are recorded in similar locations quantifying the impact of the new configuration on the transient response of the system. The results are presented using comparative graphical methods. The investigation is performed based on the electromagnetic field theory approach: the PEEC method, previously described and was successfully implemented under XGSLab software interface [49]. A typical GIS grounding grid is assessed using a novel methodology proposed by the authors, partially developed in [51] taking into consideration both underground and aboveground metallic interconnected conductors. The proposed methodology can be easily extended to any GIS configuration and adjacent earthing systems as well as to any fault scenario (the software package allows the injection of fault current/voltage at any location across the system).

When a fault at power frequency is considered, the total fault current discharged into the grounding grid by the metallic enclosure will dissipate towards the outer contours of the grid, whereas during very fast transients the effective area of the grid is significantly reduced. The effective area of the grid is investigated running several simulation processes considering only particular parts of the earthing system. For example, in the first instance, the vertical rods system is excluded during the computational process followed by exclusion of other particular metallic structures defined below:

- **Configuration 1:** contains the grounding grid located inside the GIS building and three copper conductor rings. Therefore, the vertical rods and the farthest copper conductor ring with respect to the GIS building, are excluded from the model (red layer, see Figure 6);

- **Configuration 2**: contains the grounding grid located inside the GIS building and two copper conductor rings are excluded from the model (red and blue layers, see Figure 6);.
- **Configuration 3**: contains the grounding grid located inside the GIS building and three copper conductor rings are excluded from the module (red, blue and purple layers, see Figure 6).
- **Configuration 4**: the grounding grid located inside the GIS building contains only the copper strip and four copper conductor rings are excluded from the model (red, orange, purple and green layers, see Figure 6).

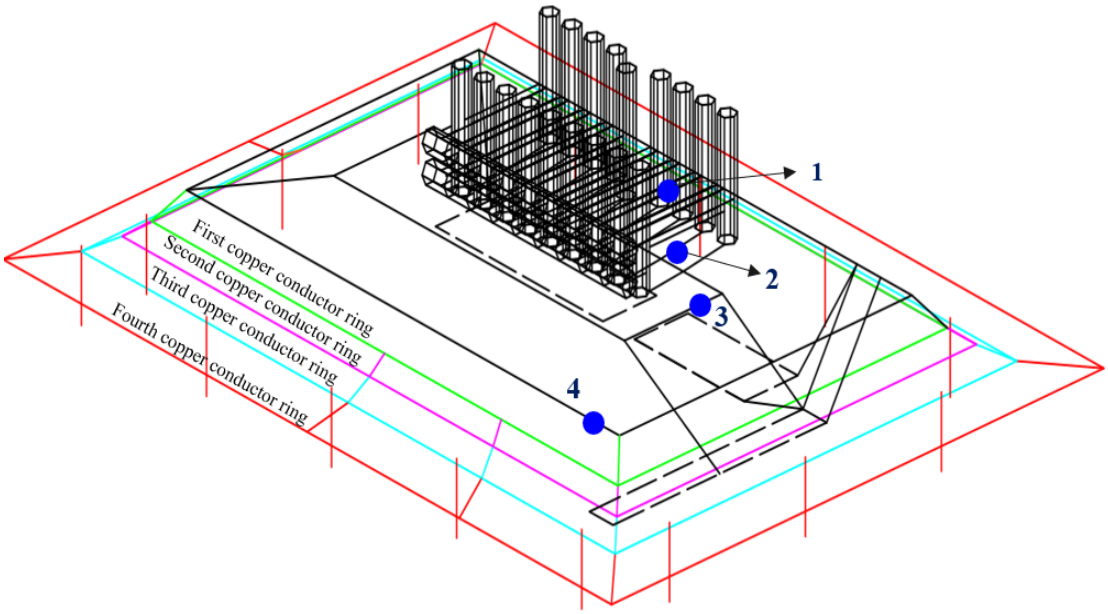

Figure 6. Locations used for analysis

Gradually, the grounding grid configuration will be simplified until *Configuration 4* is achieved. Several important locations for analysis are established inside the GIS building. For example, on the upper side of BS6 enclosure (horizontal side) *Location 1*; on the grounding lead which connects the BS6 enclosure to the grounding system, *Location 2*; on a copper strip located on the GIS concrete platform, *Location 3*; and finally on a copper strip located on the inner wall of the GIS building, *Location 4* (see Figure 6).

IV. RESULTS

A. Assessment of accurate transient response of the GIS during voltage breakdown fault

In the following section, based on the information regarding the adopted modeling scenarios presented in previous sections, the Transient Ground Potential Rise, using PEEC electromagnetic field approach methodology, across the GIS building and the metallic enclosure is computed and discussed.

In order to provide an accurate representation of the TGPR behavior during switching events across the GIS building, a three-dimensional illustration of the TGPR across the GIS building is presented and discussed, see Figure 7. Through data processing techniques the overall transient behavior of the substation is represented considering 1000 data points obtained by exporting the per-fault-unit ($p.f.u.$) values describing the transient voltage from the XGSLab software package linked with the Cartesian coordinates system containing the x, y, and z coordinates for each individual element. In order to be able to represent the TGPR spatial distribution inside of the GIS building as accurately as possible 100 locations across the grounding grid and metallic enclosure are established for the purpose of analysis. During the assessment of safety criteria related to a certain substation, several parameters describing the transient regime require special attention:

a) The maximum amplitude of the TGPR;
b) The temporal distribution of the TGPR (rise time parameter)

An interpolation algorithm is used to ensure transition from one subsystem to another across the substation (mesh configuration) is achieved.

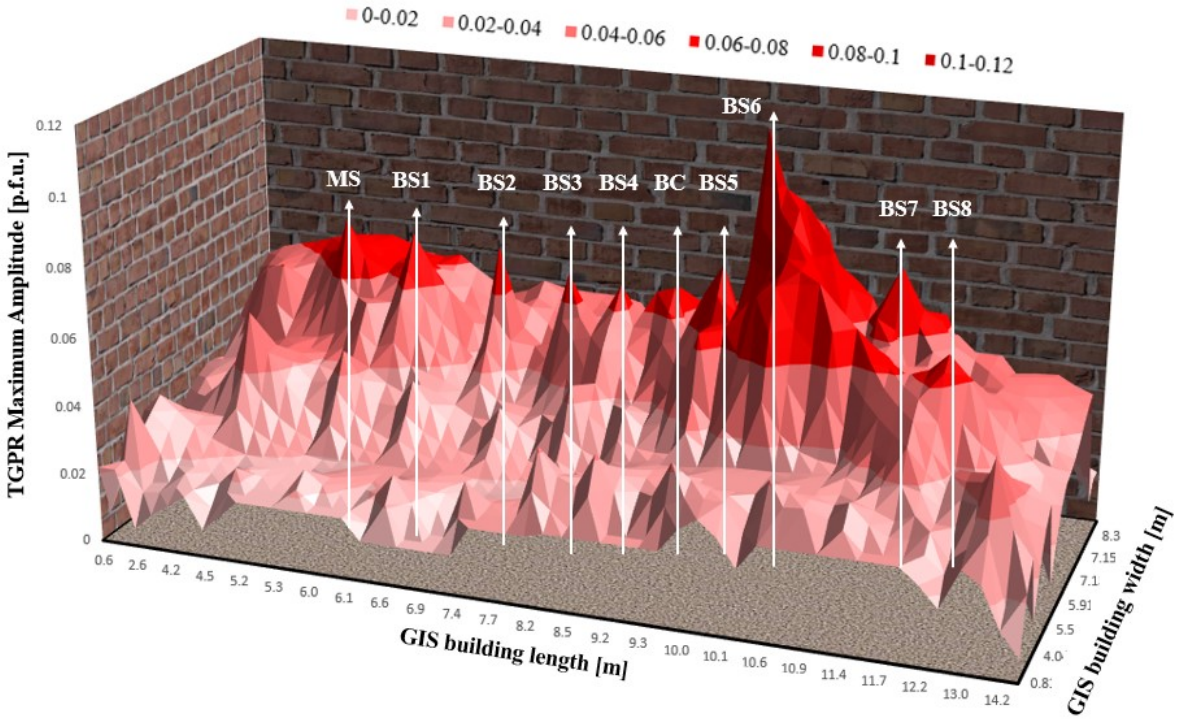

Figure 7. Three-dimensional representation of TGPR amplitude across GIS building

Figure 7 illustrates the spatial distribution of the transient ground potential rise inside of the GIS building or housing.

The rise time characterizing the steepness of TGPR waveforms is illustrated in Figure 8. In order to be able to provide a graphical illustration of the rise time parameter (in which certain TGPR waveforms reach maximum amplitudes) a reference value is established. By means of data processing techniques, the maximum value of the rise time parameter was extracted from the data set. Each particular time value presented in Figure 8 represents the difference between the

reference value ($2.4\,\mu s$) and the real value describing the waveform steepness. As the electromagnetic wave circulates or travels along the path provided by the metallic structures contained by the model, a delay of the wave reaching the maximum amplitude can be observed. The steepest waveforms are computed close to the transient source on the metallic enclosure related with the fault location (breakdown voltage). However, due to reflections and refractions of the wave phenomena (especially when the electromagnetic wave is reaching the end of the traveling path) steeper voltage waveforms can be observed along the GIS enclosure.

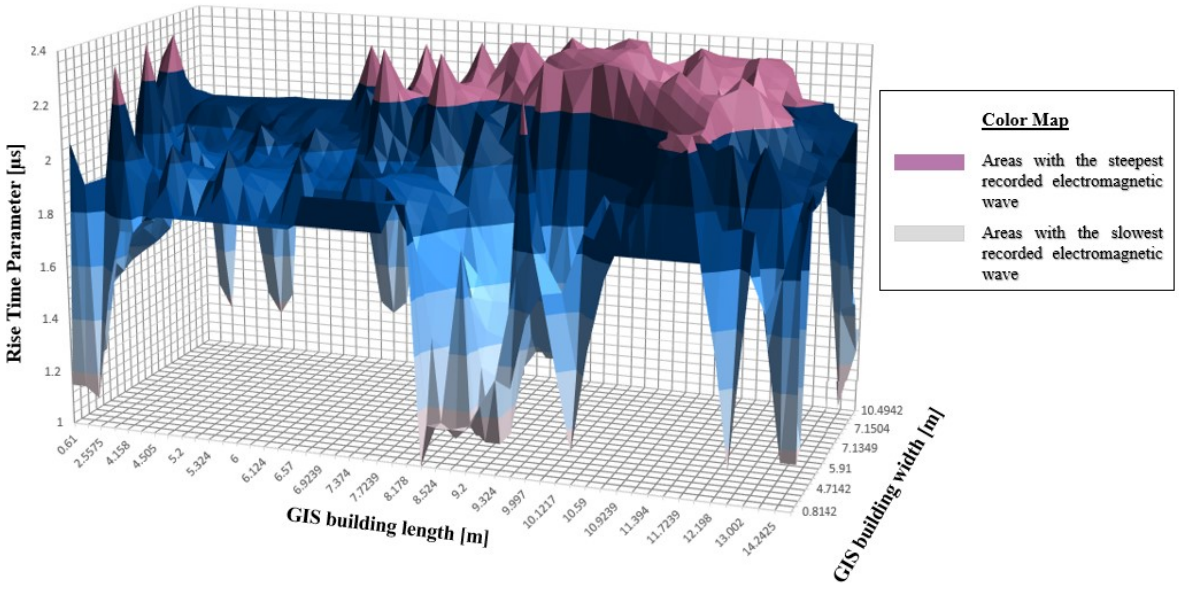

Figure 8. Spatial distribution of the rise time parameter describing the TGPR waveforms across the substation

As the distance between the transient source and the location under analysis increases, the amplitude of the transient potential considerably decreases due to the resultant electromagnetic couplings developed between the metallic structures contained by the system under study and the damping effect provided by the grounding grid. Furthermore, the intensity of wave attenuation phenomenon (from an amplitude point of view) increases with the distance from VFTO source as shown in Figure 7.

The TGPR evolution across the GIS building, presented in Figure 7, raises the question of how the grounding grid impacts the transient overvoltage flowing throughout the substation and which particular sub-systems acts efficiently in attenuating the Transient Ground Potential Rise. In this regard, a further step-by-step analysis is employed in order to identify the critical grounding grid sub-systems during VFTO phenomenon. Finally, a mitigation technique is proposed which successfully attenuates the TGPR at the level of the GIS building.

B. Step-by-step analysis applied to transient behavior of GIS, considering several configurations of the grounding system

In the following section the impact of certain sub-systems of the grounding grid on TGPR across the substation is analyzed, following the assessment procedure discussed previously.

Figures 9-11 show the computed TGPR considering several grounding grid configurations at *Locations 1*, *2*, *3* and *4* respectively. The summary of findings is shown in Table 4. For each simulation, the complete configuration of the grounding grid is considered as the baseline. Also, the computed TGPR is a consequence of a voltage breakdown fault inside BS6 enclosure.

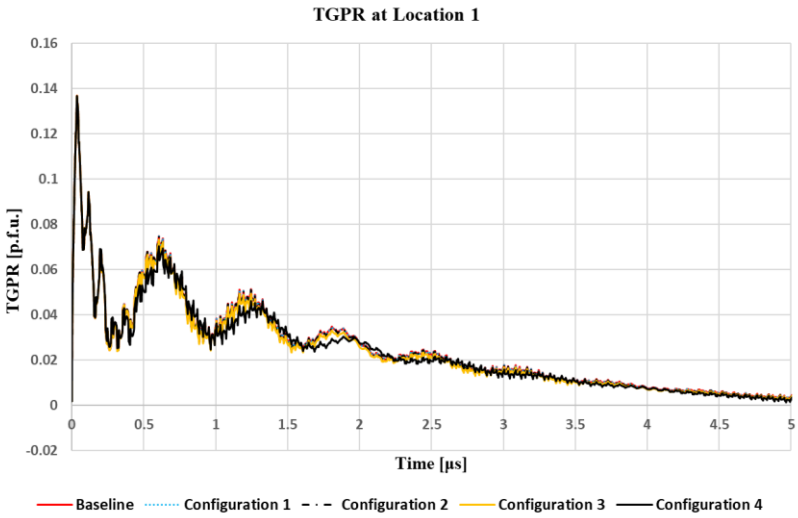

Figure 9. TGPR computed considering several grounding grid configurations at Location 1

Table 4. Parameters describing the TGPR for different grounding grid configurations

Analysis point	Considered Parameter	Entire model	Configuration 1	Configuration 2	Configuration 3	Configuration 4
1	Max Voltage [p.f.u.]	0.136721	0.1367719	0.136714	0.136682	0.136569
2	Max Voltage [p.f.u.]	0.079924	0.0799927	0.079918	0.079902	0.07979
3	Max Voltage [p.f.u.]	0.030338	0.030362	0.030344	0.030398	0.030452
4	Max Voltage [p.f.u.]	0.022503	0.02587	0.024138	0.026966	0.037088
	Percentage differences [%]		0.40 %	6.86 %	11.72 %	37.52 %

It is important to note that the resultant electromagnetic wave illustrated throughout the paper contains incident, reflected and refracted components.

While the analysis location is set further with respect of transient source, the maximum computed amplitude of the TGPR at Location 2 decreases by 57 % considering $1.2\ m$ distance from *Location 1*. If the maximum amplitudes of TGPR computed at analysis point 2 and 3 are compared an attenuation rate of 37.5 % is obtained, see Table 4, meaning that an important attenuation rate is achieved considering very short distances. The total length of acceptable earthing system simplifications of the computational domain during the simulation process is 67 % with respect to the total physical length of the grid metallic conductors. The aforementioned

conclusion can be extended also to steady-state regime when the levels of transient enclosure voltage can reach up to $0.7\ p.u.$ [22].

Differently from the physical phenomenon occurring at power frequency fault when the fault currents tend to flow through the external contours of the earthing system, during very fast transients, the maximum amplitudes of the electromagnetic wave are recorded within the grounding system located beneath the GIS enclosure. Regarding the results computed when different configurations of the grounding grid are tested and similar behavior of the TGPR with maximum amplitudes and time distributions are recorded at *Location 2* and *3* although important simplification of the computational domain are achieved.

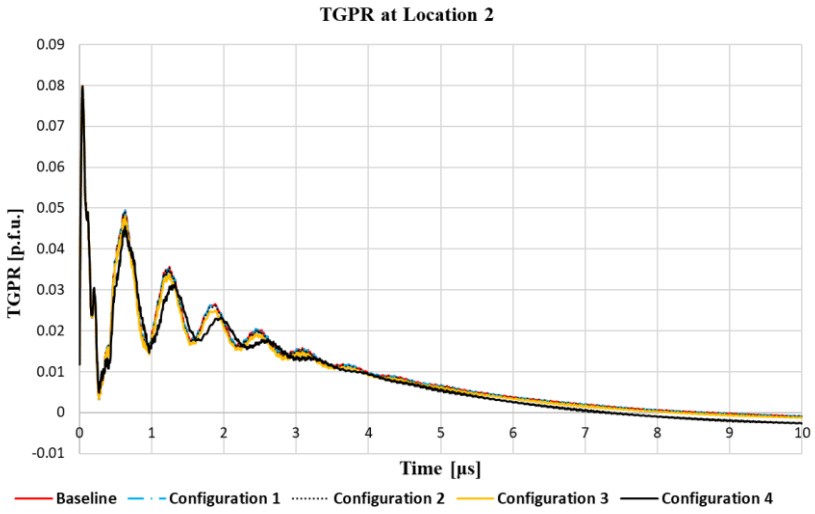

Figure 10. TGPR computed considering several grounding grid configurations at Location 2

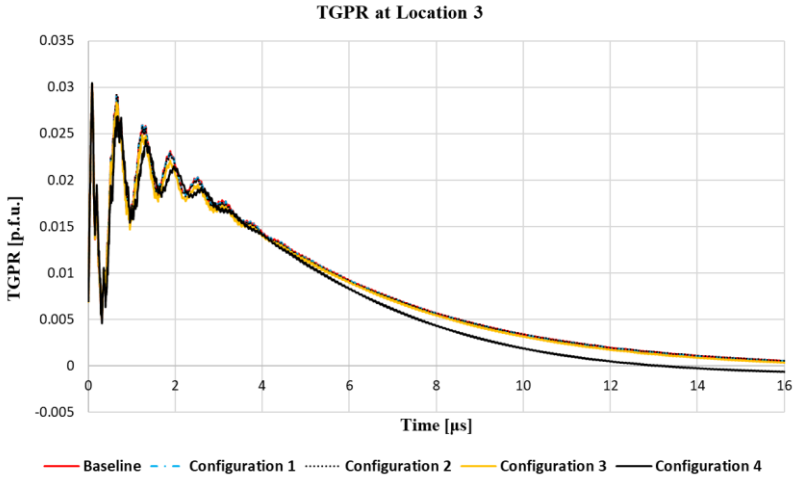

Figure 11. TGPR computed considering several grounding grid configurations at Location 3

Whilst the analysis is performed at *Location 4*, on the copper strip contour located on the GIS building inner wall, an increase of 37.52 %, in the TGPR amplitude is observed with *Configuration 4*. Based on the previous observations one can state that the TGPR generated at the

level of GIS platform during a phase-to-enclosure fault cannot be suppressed through mitigation techniques applied on the outer contours of the grounding grid located outside of the GIS building although it would be easier to implement from a constructive point of view.

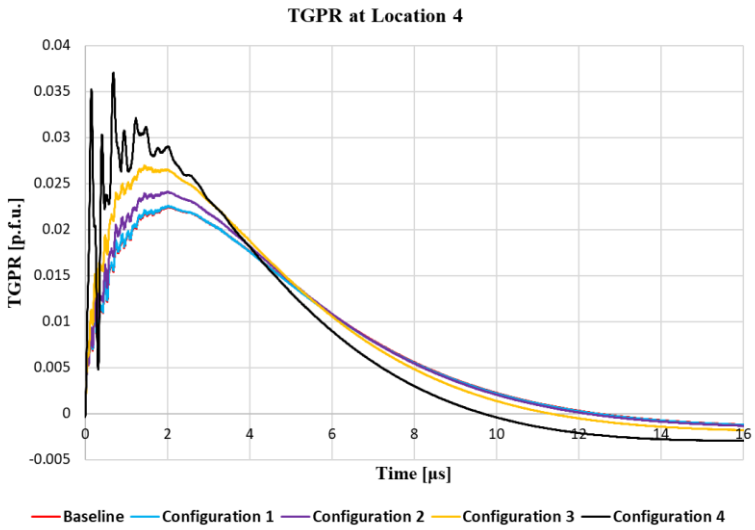

Figure 12. TGPR computed considering several grounding grid configurations at Location 4

If the recorded TGPR at analysis *Location 1* and *Location 4* are compared, an attenuation rate of 85% is obtained meaning that the transient electromagnetic wave is mostly cleared before reaching the copper strip contours located outside of the GIS building. Taking into account the grounding grid *Configuration 4* an oscillatory character of the voltage time domain waveform occurs, differently as when the first three grounding grid configurations are considered, see Figure 12.

When the transient current at *Locations 1*, *2*, *3* and *4* is computed, a similar response of the earthing system as in previous cases is observed, see Table 5.

Table 5. Numerical analysis regarding recorded transient current

Analysis Location	Considered Parameter	Entire model	Configuration 1	Configuration 2	Configuration 3	Configuration 4
1	Max Current [p.f.u]	0.010782	0.010782	0.010785	0.010791	0.010796
2	Max Current [p.f.u]	0.020641	0.020641	0.020635	0.020637	0.020642
3	Max Current [p.f.u]	0.007426	0.007426	0.007407	0.007414	0.007440
4	Max Current [p.f.u]	0.002775	0.002769	0.002732	0.001991	0.002541

Similar maximum amplitudes, time distributions and clearance time of the transient current waveform recorded considering simplification of the grounding grid are observed. It is important to mention that the transient source is modeled through an ideal EMF generator therefore the transient current flowing throughout the system is a consequence of the characteristic impedance

of the propagation path as well as to the aforementioned electromagnetic couplings. When the physical length of the grounding grid is reduced by subtracting the buried copper conductors located outside of the GIS building, the topology of the transient current waveform computed at *Location 4* is considerably affected. Although the peak current amplitudes are higher considering the baseline for *Configurations 1*, *2* and *3*, the performance of the earthing system is considerably reduced when *Configuration 4* is adopted.

The numerical results obtained at *Locations 1*, *2* and *3* are not dependent on the outer grounding grid sub-systems. However, significant differences between computed results arise at *Location 4* where the grounding grid *Configurations 3* and *4* are considered, see Table 5. When the maximum amplitudes of the transient current computed near the transient source and on the copper strip located on the inner wall of GIS building are compared, an attenuation rate of 440 % is obtained meaning that the fault current is mostly attenuated within the grounding grid located beneath GIS enclosure. In general, even if harmful levels of transient currents and voltages occur throughout GIS substation due to fault current leakage towards the grounding system, the transient electromagnetic waveform will be mostly attenuated before reaching the physical ends of the earthing system. Therefore, modifications of the grounding grid will be implemented on the GIS platform in order to quantify the impact on TGPR variations. In the following section the topology of the grounding grid located beneath the GIS enclosure is modified in order to endorse the previous stated conclusion.

C. Mitigation Technique from a constructive point of view

From a theoretical point of view, it is necessary to use an equipotential grid in order to accurately attenuate the effects of very fast transients that occur when switching operations in GIS are conducted. Besides the voltage breakdown fault scenario, the switching transients leak towards the grounding system in the HV cable GIS transition points. In general, GIS manufactures and IEEE 80-2013 Std. [19] strongly recommend connecting the metallic enclosure to the earthing system at least in two locations using a short grounding lead. In [21] a grounding grid design EMF method is presented however the equipotential grid located beneath the GIS enclosure which is responsible for controlling very fast transients is built with several assumptions. The proposed modeling method provides the capability not only to model the entire metallic conductors' configuration but also the performance of the grid in the presence of the metallic enclosure. The following diagram (Figure 13) shows that the density of the copper strip conductor at the GIS platform level is increased. This leads to increase in the overall cost of the grid. However, the tradeoff is for obtaining better attenuation rates across the substation, see Table 6

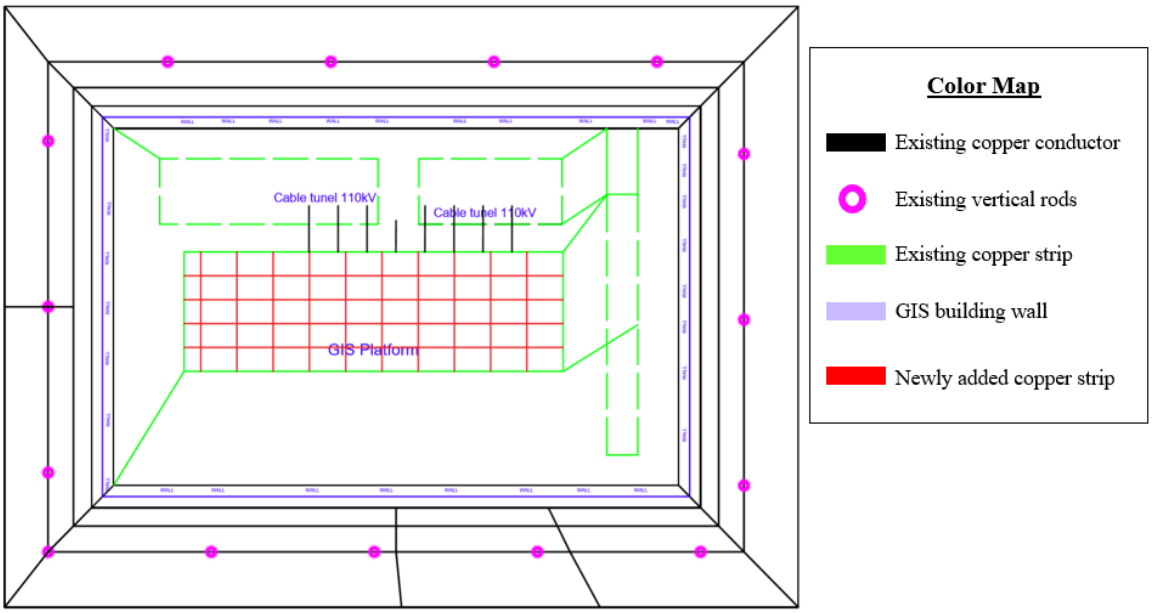

Figure 13. Modified grounding grid configuration

Furthermore, by installing a denser grid beneath the GIS enclosure the impulse impedance of the system will decrease and an equipotential surface on the GIS concrete platform can be achieved.

Table 6. Attenuation rates across the grounding grid

Analysis point	Maximum Amplitude	Initial scenario	Mitigation scenario	**Attenuation**
Location 1	TGPR [p.f.u.]	0.13672	0.11593	**15.20 %**
Location 2	TGPR [p.f.u.]	0.07992	0.02435	**69.53 %**
Location 3	TGPR [p.f.u.]	0.03034	0.01697	**44.05 %**
Location 4	TGPR [p.f.u.]	0.02250	0.00420	**81.35 %**
Location 1	Transient Current [p.f.u.]	0.01078	0.01054	**2.26 %**
Location 2	Transient Current [p.f.u.]	0.02064	0.01282	**37.91 %**
Location 3	Transient Current [p.f.u.]	0.00743	0.00091	**87.76 %**
Location 4	Transient Current [p.f.u.]	0.00277	0.00085	**69.78 %**

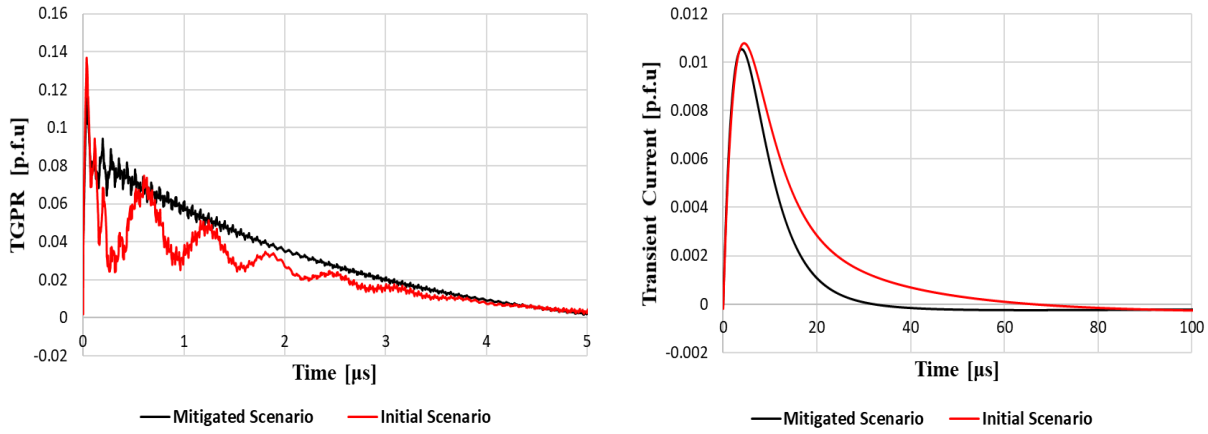

Figure 14. Mitigation technique effects at Location 1

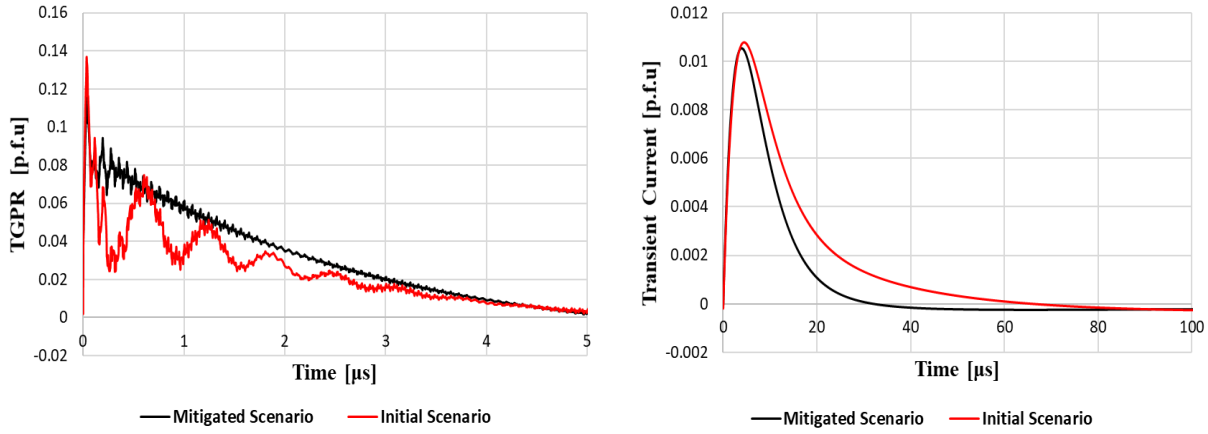

Figure 14 suggests that the lowest attenuation rates are computed on the metallic enclosure. When the observation point moves towards the grounding system, important attenuation rates are obtained proving the efficiency of the newly implemented configuration, as expected. The additional copper conductors inserted into the model are equivalent to increasing the number of current paths across the GIS platform. Moreover, due to the multiple parallelism conditions between the different sides of the metallic mesh inductive capacitive and galvanic couplings will be developed which will impact the overall performance of the system.

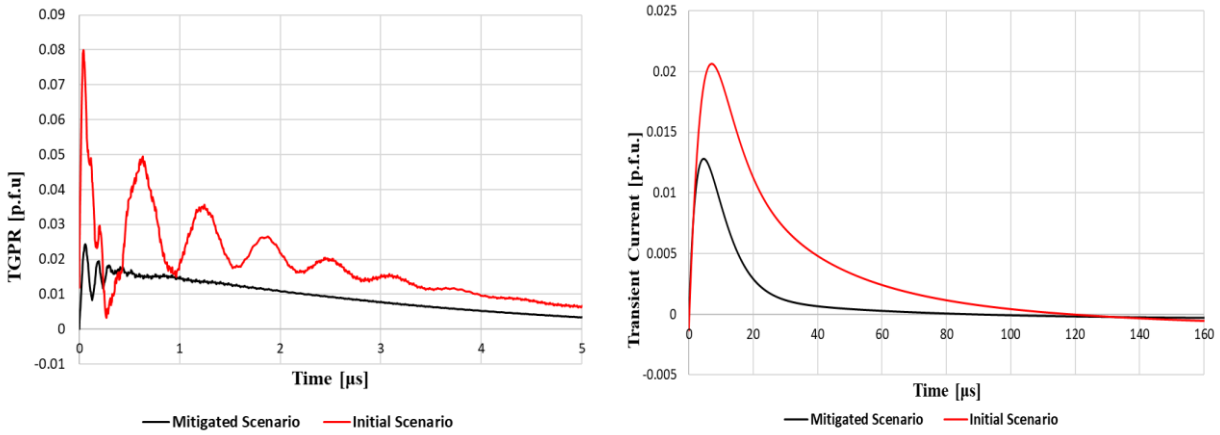

Figure 15. Mitigation technique effects at Location 2

Figure 15 illustrates the TGPR computed at *Location 2*. The oscillatory character of the TGPR waveform is considerably reduced when a denser mesh of the grounding grid is implemented. If hypothetically the system is replaced by primary circuit elements, it can be stated that its equivalent inductance, capacitance and resistance behaves as a filter. Figure 16 and Figure 17 illustrates the damping effect of the proposed grounding grid configuration highlighted through comparison means, at analysis *Locations 3* and *4*.

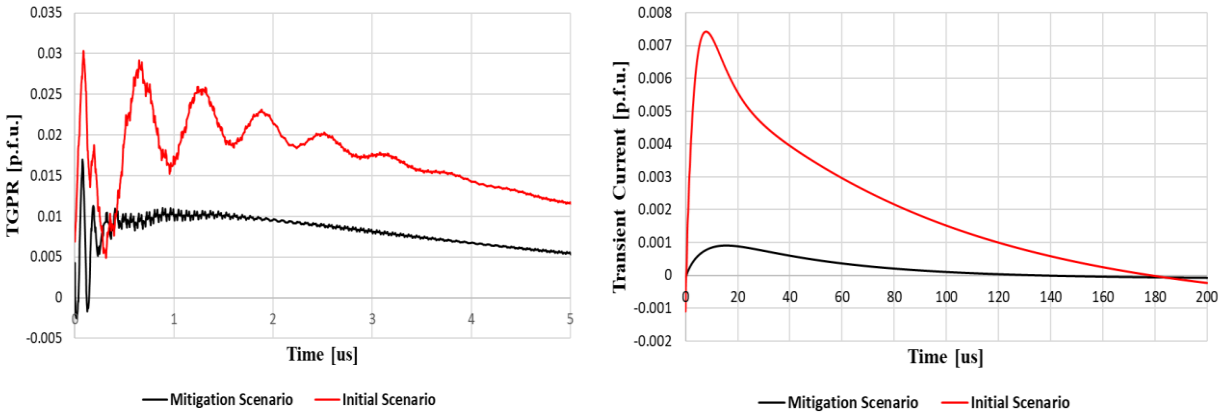

Figure 16. Mitigation technique effects at Location 3

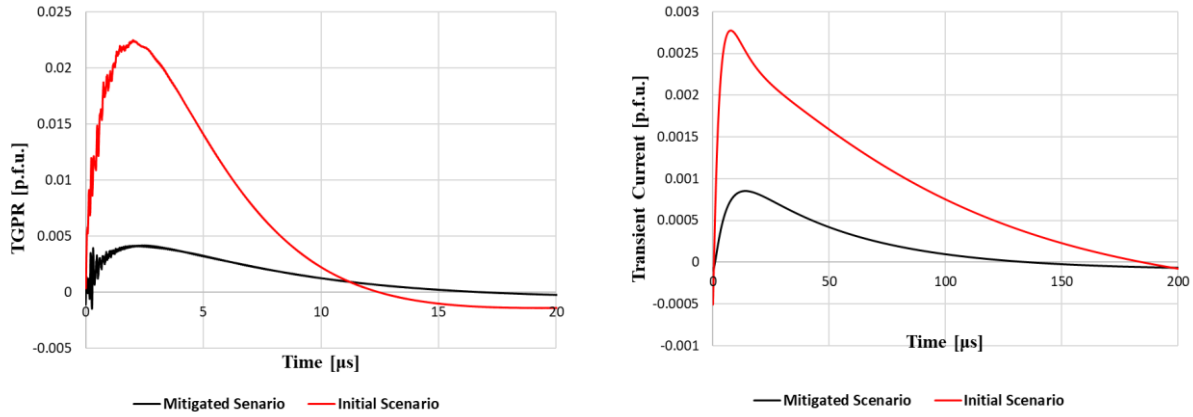

Figure 17. Mitigation technique effects at Location 4

The efficiency of the adopted grid mesh can be observed also when the observation point moves further with respect of the transient source: 44% of the TGPR and 87% of the transient current at analysis point 3 and 81% of the TGPR and 70% of the transient current at analysis *Location 4*.

V. CONCLUSIONS

The outcome of the proposed methodology provides valuable information regarding the holistic transient response of a real configuration of a Gas Insulated Substation. By proposing an effective assessment methodology, a proper mitigation technique is validated and a contribution has been added regarding the quantification of the grounding grid performance under very fast transient overvoltage. The results show how to identify the effective area of the grounding grid under the action of VFTO which is discussed below:

- By means of 3D surface plots, the holistic transient response of the system at very high frequency is evaluated during voltage breakdown fault. Maximum amplitudes of the Transient Ground Potential Rise is greater near the transient source as well as the sharpness of the electromagnetic waveforms.

- When the substation is subjected to very high frequency transient, the severity of the transient regime rapidly decreases when the analysis point moves further from the transient source. Comparison of the maximum computed amplitude of TGPR at *Location 1* and *Location 4* show a 520% attenuation rate.
- The transient electromagnetic wave attenuates within the grounding grid located beneath the GIS enclosure, before reaching the outer copper conductors rings.
- The grounding grid subsystem responsible for clearance of fault energy has been successfully identified following the step-by-step analysis: on each computational step a different grounding grid simplification has been considered.
- By applying a denser mesh on the grid located beneath the GIS enclosure optimum TGPR and transient current attenuation rates are achieved.
- By reducing the total length of the analyzed grounding grid, the required computational time and effort is significantly reduced. Despite the significant differences arising at analysis *Location 4* when grounding grid *Configurations 3* and *4* are considered, the TGPR and transient current maximum amplitudes and time distributions are not affected when one evaluates the performance of the GIS platform earthing system.
- The acceptable reduction length of the system for simplification purposes achieved during this study is 67%.

ACKNOWLEDGEMENT

This work was supported by a grant of the Ministry of Education and Research, CNS/CCDI-UEFISCDI, project number PN-III-P3-3.6-H2020-2020-0129/PPH no.44/2021

Alexandru Muresan: Conceptualization, Methodology, Validation, Investigation, Writing - Original Draft;

Levente Czumbil: Conceptualization, Validation, Formal analysis, Data Curation, Writing - Second Draft; Visualization;

Alexis Polycarpou: Formal analysis, Writing - Review & Editing, Supervision;

Hassan Nouri: Conceptualization, Formal analysis, Investigation, Writing - Review & Editing, Supervision;

Roberto Andolfato: Formal analysis, Validation, Writing - Review & Editing, Supervision;

Dan Doru Micu: Formal analysis, Investigation, Writing - Review & Editing, Supervision, Project administration, Funding acquisition.

REFERENCES

[1] G. Mazzanti, G. Stomeo & S. Mancini: "State of the Art in Insulation of Gas Insulated Substations: Main Issues, Achievements, and Trends", *IEEE Electrical Insulation Magazine*, ISSN: 0883-7554, vol. 32, no. 5, pp. 18-31, **2016**. Doi: 10.1109/MEI.2016.7552373

[2] K. Pohlink, E. Mikes & P. Ponchon: "New Aspects of Reliability in Gas Insulated Substations", *IEEE Power Engineering Society General Meeting*, Montreal, Canada, June 18-22, **2006**. Doi: 10.1109/PES.2006.1709523

[3] E. Laruelle, A. Ficheux, Y. Kieffel & I. Huet: "Environmental Impact Comparison Between a 220 kV Gas-Insulated Substation and a 220 kV Air-Insulation Substation", *IEEE Power & Energy Society General Meeting*, Vancouver, Canada, July 12-21, **2013**. Doi: 10.1109/PESMG.2013.6672384

[4] CIGRE Working Group 33/13-09: "Very Fast Transient Phenomena Associated with Gas Insulated Substations", Ref. no. 33-13_1988, CIGRE Session, August 28 – September 3, **1988**.

[5] Z. Zhongyuan, L. Guishu & C. Xiang: "The Setting Up of Conductive Coupling Model in Gas Insulated Substation", *Proceedings. International Conference on Power System Technology*, Kunming, China, October 13-17, **2002**. Doi: 10.1109/ICPST.2002.1047262

[6] IEC 60071-4, *Insulation Co-Ordination - Part 4: Computational Guide to Insulation Co-Ordination and Modelling of Electrical Networks*, ICS Code: 29.080.30, June, **2004**.

[7] M. Babaei, S. Addelwahed & M. Babaei: "Transient Ground Potential Rise in Gas Insulated Substations and Analysis of Effective Factors", *ASME Power Conference*, San Diego, USA, June 28 - July 2, **2015**. Doi: 10.1115/POWER2015-49597

[8] T. Chen, H. Liu, D. Hu, X. Liu, T. Xu, X. Yang & L. Ji Liang: "Shell Circulating Current and Transient Ground Potential Rise in 220 kV GIS", *The Journal of Engineering*, ISSN: 2051-3305, vol. 2017, no. 13, pp. 2555-2558, **2017**. Doi: 10.1049/joe.2017.0788

[9] M.A. Haseeb & M.J. Thomas: "Disconnector Switching Induced Transient Voltage and Radiated Fields in a 1100 kV Gas Insulated Substation", *Electric Power Systems Research*, ISSN: 0378-7796, vol. 161, pp. 86-96, August, **2018**. Doi: 10.1016/j.epsr.2018.04.001

[10] S. Rahmani & A.A. Razi-Kazemi: "Investigation of Very Fast Transient Overvoltages in Gas Insulated Substations", *2nd International Conference on Knowledge-Based Engineering and Innovation*, Teheran, Iran, November 5-6, **2015**. Doi: 10.1109/KBEI.2015.7436083

[11] H. Xue, A. Ametani & J. Mahseredjian: "Very Fast Transients in a 500 kV Gas-Insulated Substation", *IEEE Transactions on Power Delivery*, ISSN: 0885-8977, vol. 34, no. 2, pp. 627-637, April, **2019**. Doi: 10.1109/TPWRD.2018.2874331

[12] D.C. Moreira, M.V.A. Nunes, D.D.C. Moreira & D.K.D. Costa: "Analysis of VFTO during the Failure of a 550 kV Gas-Insulated Substation", *Electric Power Systems Research,* ISSN: 0378-7796, vol. 189, art. no. 106825, **2020**. Doi: 10.1016/j.epsr.2020.106825

[13] D.T.A Kho & K.S. Smith: "Analysis of Very Fast Transient Overvoltages in a Proposed 275 kV Gas Insulated Substation", *International Conference on Power Systems Transients (IPST)*, ISSN: 2434-9739, Delft, the Netherlands, June 14-17, **2011**. (link)

[14] M.M. Rao, M.J. Thomas & B.P. Singh: "Frequency Spectrum Analysis of Fast Transient Currents (FTC) due to Switching Operations in a 245 kV GIS", *IEEE/PES Transmission and Distribution Conference and Exhibition*, Yokohama, Japan, October 6-10, **2002**. Doi: 10.1109/TDC.2002.1177812

[15] A. Raghu Ram, J. Amarnath, S. Kamakshiah: "Estimation of Very Fast Transient Overvoltages on Bushing Connected in GIS", *Internation Journal of Engineering Science and Technology (IJEST)*, ISSN: 2278-9510, vol 4, no. 2, pp. 457-472, February, **2012**. (link)

[16] M. Kondalu & P.S. Subramanyam: "Estimation of Re-Striking Transient Over Voltages in a 132KV Gas Insulated Substation", *International Electrical Engineering Journal (IEEJ)*, ISSN: 2078-2365, vol. 3 , no. 2, pp. 757-763, **2012**. (link)

[17] B. Liu, Y. Tong, X.P. Deng & X.X. Feng: "Measuring of Very Fast Transient Overvoltage and Very Fast Transient Current Generated by Disconnector Operating", *International Conference on Power System Technology (POWERCON)*, Chengdu, China, October, 20-22, **2014**. Doi: 10.1109/POWERCON.2014.6993660

[18] Y. Cai, Y. Guan & W. Liu, "Measurement of Transient Enclosure Voltage in a 220kV Gas Insulated Substation", *IEEE International Instrumentation and Measurement Technology Conference (I2MTC)*, Pisa, Italy, May 11-14, **2015**. Doi: 10.1109/I2MTC.2015.7151250

[19] IEEE Std. 80, *IEEE Guide for Safety in AC Substation Grounding*, ICS Code: 29.120.50, May, **2015**. Doi: 10.1109/IEEESTD.2015.7109078

[20] B.R. Gupta & V.K. Singh: "Impulse Impedance of Rectangular Grounding Grid", *IEEE Transactions on Power Delivery*, ISSN: 0885-8977, vol. 7, no. 1, pp. 214- 218, January, **1992**. Doi: 10.1109/61.108910

[21] M. Tello, G.A.D. Dias, D.S. Gazzana, R.C. Leborgne & A.S. Bretas: "EMC Philosophy applied to Design the Grounding Systems for Gas Insulation Switchgear (GIS) Indoor Substation", *15th International Conference on Environment and Electrical Engineering (EEIC)*, Rome, Italy, June 10-13, **2015**. Doi: 10.1109/EEEIC.2015.7165200

[22] A.A. Razi-Kazemi: "Numerical Simulation and Analytical Calculation of the GIS Transient Enclosure Voltage Interaction with Grounding System", *Electric Power Systems Research*, ISSN: 0378-7796, vol. 194, art. no. 107123, **2021**. Doi: 10.1016/j.epsr.2021.107123

[23] P. Yutthagowith, A. Ametani, N. Nagaoka & Y. Baba: "Application of the Partial Element Equivalent Circuit Method to Analysis of Transient Potential Rises in Grounding Systems" *IEEE Transactions on Electromagnetic Compatibility*, ISSN: 0018-9375, vol. 53, no. 3, pp. 726-736, August, **2011**. Doi: 10.1109/TEMC.2010.2077676

[24] D. Povh, H. Schmitt, O. Volcker, R. Witzmann, P. Chewdhuri, A.E. Imece, R. Iravani, J.A. Martinez, A. Keri & A. Sars: "Modeling and Analysis Guidelines for Very Fast Transients", *IEEE Power Engineering Review*, ISSN: 0272-1724, vol. 16, no. 10, October, **1996**. Doi: 10.1109/MPER.1996.4311053

[25] D. Povh, H. Schmitt, O. Volcker & R. Witzmann: "Modeling and Analysis Guidelines for Very Fast Transients ", *IEEE Transactions on Power Delivery*, ISSN: 0885-8977, vol. 11, no. 4, pp 2028-2035, October, **1996**. Doi: 10.1109/61.544291

[26] T. Kuczek & M. Florkowski: "Modeling of Overvoltages in Gas Insulated Substations", *Przeglad Elektrotechniczny*, ISSN: 0033-2097, vol. 04a/2012, pp. 305-308, **2012**. (link)

[27] CIGRE Working Group C4.501, *Guideline for Numerical Electromagnetic Analysis Method and its Application to Surge Phenomena*, CIGRE Technical Brochures, ISBN: 978-2-85873-237-1, Ref. no. 543, **2013**. (link)

[28] J. Liu, F.P. Dawalibi & B.F. Majerowicz: "Gas Insulated Substation Grounding System Design using the Electromagnetic Field Method", *China International Conference on Electricity Distribution*, Shanghai, China, September 10-14, **2012**. Doi: 10.1109/CICED.2012.6508717

[29] F.P. Dawalibi, M.A. Joyal, J. Liu & Y. Li: "Realistic Integrated Grounding and Electromagnetic Interference Analysis Accounting for GIS, Cables and Transformers During Normal and Fault Conditions", *IEEE PES Asia-Pacific Power and Energy Engineering Conference (APPEEC)*, Hong Kong, China, December 8-11, **2013**. Doi: 10.1109/APPEEC.2013.6837307

[30] Z. Jinsong, Q. Feng, G. Bing, Y. Li & F.P. Dawalibi: "*Grounding of Urban GIS Substation Connected to Commercial Buildings and Metallic Infrastructures*", *International Journal of Materials, Mechanics and Manufacturing (IJMMM)*, ISSN: 1793-8198, vol. 3, no. 3, pp. 191-196, August, **2015**. Doi: 10.7763/IJMMM.2015.V3.194

[31] W. Xin, G. Zhang, W. Yuan, J. Wu & Y. Geng: "Calculation of Transient Electromagnetic Fields Generated during Switching Operation in Power Substation by the Method of Moment and Superposition Principle", *2nd International Conference on Electric Power Equipment - Switching Technology (ICEPE-ST)*, Matsue, Japan, October 20-23, **2013**. Doi: 10.1109/ICEPE-ST.2013.6804385

[32] D. Pommerenke & S. Sakaguchi: "Application of Maxwell Solvers to PD Propagation. I. Concepts and Codes", *IEEE Electrical Insulation Magazine*, ISSN: 0883-7554, vol. 18, no. 5, **2002**. Doi: 10.1109/MEI.2002.1044317

[33] S. Sakaguchi, M. Oyama "Application of Maxwell Solvers to PD Propagation. III: PD Propagation in GIS", *IEEE Electrical Insulation Magazine*, ISSN: 0883-7554, vol. 19, no.1, **2003**. Doi: 10.1109/MEI.2003.1178103

[34] J. Smajic, W. Holaus, J. Kostovic & U. Riechert, "3D Full-Maxwell Simulations of Very Fast Transients in GIS", *IEEE Transactions on Magnetics*, ISSN: 018-9464, vol. 47, no. 5, pp. 1514-1517, May, **2011**. Doi: 10.1109/TMAG.2010.2090653

[35] J. Smajic, A. Shoory, S. Burow, W. Holaus, U. Riechert & S. Tenbohlen: "Simulation-Based Design of HF Resonators for Damping Very Fast Transients in GIS", *IEEE Transactions on Power Delivery*, ISSN: 0885-8977, vol. 29, no. 6, pp. 2528-2533, December, **2014**. Doi: 10.1109/TPWRD.2014.2330757

[36] M. Szewczyk, W. Piasecki, M. Wroński & K. Kutorasiński: "New Concept for VFTO Attenuation in GIS with Modified Disconnector Contact System", *IEEE Transactions on Power Delivery*, ISSN: 0885-8977, vol. 30, no. 5, pp. 2138-2145, October, **2015**. Doi: 10.1109/TPWRD.2014.2377094

[37] M. Szewczyk, K. Kutorasiński, M. Wroński & M. Florkowski: "Full-Maxwell Simulations of Very Fast Transients in GIS: Case Study to Compare 3-D and 2-D-Axisymmetric Models of 1100 kV Test Setup", *IEEE Transactions on Power Delivery*, ISSN: 0885-8977, vol. 32, no. 2, pp. 733-739, April, **2017**. Doi: 10.1109/TPWRD.2016.2527823

[38] B. Florkowska, P. Zydron & A. Jackowicz-Korczynski: "Electric Field Modelling in Gas-Insulated Substation for Analysis of Conditions for Partial Discharge Phenomena", *Acta Physica Polonica*, ISSN: 1898-794X, vol. 12, no. 3, pp. 319-325, **2015**. Doi: 10.12693/APhysPolA.128.319

[39] B. Lu, Y. Shi, X. Lin & X. Bian: "3D Full Maxwell Research for Effect of Initial Electromagnetic Field on Very Fast Transient Overvoltage in GIS", *IEEE Transactions on Dielectrics and Electrical Insulation*, ISSN: 1070-9878, vol. 23, no. 6, pp. 3319-3327, December, **2016**. Doi: 10.1109/TDEI.2016.005390

[40] M. Hikita,S. Ohtsuka, S. Okabe, J. Wada, T. Hoshino & S. Maruyama: "Influence of Disconnecting Part on Propagation Properties of PD-Induced Electromagnetic Wave in Model GIS", *IEEE Transactions on Dielectrics and Electrical Insulation*, ISSN: 1070-9878, vol. 17, no. 6, December, **2010**. Doi: 10.1109/TDEI.2010.5658223

[41] M. Hikita, S. Ohtsuka, J. Wada, S. Okabe, T. Hoshino & S. Maruyama: "Study of Partial Discharge Radiated Electromagnetic Wave Propagation Characteristics in an Actual 154 kV Model GIS", *IEEE Transactions on Dielectrics and Electrical Insulation*, ISSN: 1070-9878, vol. 19, no. 1, pp. 8-17, February, **2012**. Doi: 10.1109/TDEI.2012.6148497

[42] K. Nishigouchi, M. Kozako, M. Hikita, T. Hoshino, S. Maruyama & T. Nakajima: "Waveform Estimation of Particle Discharge Currents in Straight 154 kV GIS using Electromagnetic Wave Propagation Simulation", *IEEE Transactions on Dielectrics and Electrical Insulation*, ISSN: 1070-9878, vol. 20, no. 6, pp. 2239-2245, December, **2013**. Doi: 10.1109/TDEI.2013.6678875

[43] H. Tanaka, D. Tanahashi, Y. Baba, N. Nagaoka, N. Okada, H. Ohki & M. Takeuchi: "Finite-Difference Time-Domain Simulation of Partial Discharges in a Gas Insulated Switchgear", *High Voltage*, ISSN: 2397-7264, vol. 1, no. 1, pp. 52-56, April, **2016**. Doi: 10.1049/hve.2016.0006

[44] A. Ametani, H. Xue, M. Natsui & J. Mahseredjian: "Electromagnetic Disturbances in Gas-Insulated Substations and VFT Calculations", *Electric Power Systems Research*, ISSN: 0378-7796, vol. 160, pp. 191-198, July, **2018**. Doi: 10.1016/j.epsr.2018.02.014

[45] R. Yao, Y. Zhang, G. Si, C. Wu, N. Yang & Y. Wang: "Simulation Analysis on the Propagation Characteristics of Electromagnetic Wave in T-Branch GIS based on FDTD", *15th Mediterranean Microwave Symposium (MMS),* Lecce, Italy, November 30 – December 2, **2015**. Doi: 10.1109/MMS.2015.7375458

[46] M.M. Rao, M.J. Thomas & B.P. Singh: "Computation of EMI Fields in a High Voltage Gas Insulated Substation during Switching Operations", *IEEE Symposium on Electromagnetic Compatibility*, Boston, USA, August 18-22, **2003**. Doi: 10.1109/ISEMC.2003.1236700

[47] M.M. Rao, M.J. Thomas & B.P. Singh: "Electromagnetic Field Emission from Gas-to-Air Bushing in a GIS During Switching Operations", *IEEE Transactions on Electromagnetic*

Compatibility, ISSN: 0018-9375, vol. 49, no. 2, pp. 313-321, May, **2007**. Doi: 10.1109/TEMC.2007.893334

[48] M.M. Rao, M.J. Thomas & B.P. Singh: "Shielding Effectiveness of the Gas-Insulated Bus Duct for Transient EM Fields Generated in a GIS during Switching Operations", *IEEE Transactions on Power Delivery*, ISSN: 0885-8977, vol. 23, no. 4, pp. 1946-1953, October, **2008**. Doi: 10.1109/TPWRD.2008.923065

[49] *XGSLab user guide 2021 version*, link.

[50] *PSCAD User's Guide v4.6*, link.

[51] A. Muresan, L. Czumbil, R. Andolfato, H. Nouri & D.D. Micu: "Novel Electromagnetic Field Theory Approach Applied to Gas Insulated Substation Transient Behavior during Lightning Surge", *Mediterranean Conference on Power Generation, Transmission , Distribution and Energy Conversion (MEDPOWER)*, Paphos, Cyprus, November 9-12, **2020**. Doi: 0.1049/icp.2021.1234

[52] A. Muresan, L. Czumbil, R. Andolfato, H. Nouri Hassan & D.D. Micu: "Investigating the Effect of Several Model Configurations on the Transient Response of Gas-Insulated Substation during Fault Events Using an Electromagnetic Field Theory Approach", *Energies*, ISSN: 1996-1073, vol. 13, no. 23, art. no. 6231, **2020**. Doi: 10.3390/en13236231